BULLETIN OF THE POLISH ACADEMY OF SCIENCES
TECHNICAL SCIENCES, Vol. 73(6), 2025, Article number: e156769
DOI: 10.24425/bpasts.2025.156769

A universal algorithm for spur gear optimization based on selective search: Numerical methodology and applications

Piotr STROJNY*

Faculty of Mechanical Engineering and Aeronautics, Rzeszów University of Technology, al. Powstańców Warszawy 12, 35-959 Rzeszów, Poland

Abstract. This paper presents a universal methodology for the numerical optimization of spur gear parameters based on the selective search method. Unlike heuristic or commercial approaches, the proposed algorithm is deterministic, easy to implement in any numerical environment, and guarantees full coverage of the feasible design space. The developed mathematical model precisely describes the tooth geometry, including the involute flank and the extended root transition curve, and was validated against CAD simulations of the generating cutting process. A novel numerical procedure was introduced to calculate tooth root stresses with sub-micron resolution, achieving excellent agreement with FEM (maximum error below 1.7%) while maintaining negligible computational cost. The main novelty of this study lies in combining simplicity and universality with high numerical accuracy. Compared to existing optimization strategies, the algorithm offers faster convergence, lower error margins, and flexibility to integrate additional constraints and decision variables. Beyond gear design, the proposed approach can be applied to lightweight mechanical structures, sustainable manufacturing, and AI-assisted digital twins. The results demonstrate that the method enables rapid and cost-effective optimization, making it suitable for early design stages where FEM-only optimization would be too expensive and time-consuming.

Keywords: gear transmission; numerical optimization; involute; finite element method (FEM); stress analysis.

1. INTRODUCTION

The optimization of gear parameters remains a major challenge in modern mechanical engineering. Classical analytical methods provide only approximate solutions, while advanced FEM-based tools, though accurate, are computationally expensive and require specialized expertise. Heuristic algorithms such as genetic algorithms, tabu search, or Bayesian optimization [1–3] offer flexible exploration of the solution space, but their probabilistic nature leads to uncertainty in convergence and may result in local optima. At the same time, recent progress in accelerating numerical solvers has reduced computational burdens for physics-based analyses [4]. What is still missing is a simple, deterministic, and universal methodology that guarantees full exploration of the feasible design space with high accuracy and low computational cost.

This study addresses that gap by proposing a methodology for the numerical optimization of spur gears with straight tooth lines, based on the selective search method. A mathematical model describing the tooth geometry was developed, accounting for both the involute flank and the extended root transition curve. In addition, a numerical procedure for the precise calculation of tooth root stresses was formulated. The obtained optimization results were validated against finite element method (FEM) simulations, while the correctness of the derived geometry was confirmed by comparison with CAD-based generating process simulations.

The existing work provides a solid foundation for this study. Dynamic modeling of gears enables analysis of tooth interactions under variable loads [5], while analytical and numerical tooth geometry modifications support parameter optimization [6, 7]. The accuracy of nonmetallic/composite gears has also been investigated, informing geometry definition and tolerancing [8].

Recent advances emphasize both computational efficiency and hybrid optimization. Improved population-based search (e.g., sparrow search) has been adapted to engineering tuning tasks [9], while topology optimization without explicit volume constraints opens new avenues for lightweight design [10].

In parallel, broader engineering applications demonstrate the relevance of efficient and generalizable optimization frameworks: optimization of plasma welding sequences [11]; meshing characteristics in precision reducers with tooth modification and manufacturing errors [12]; high-fidelity propulsion system modeling for drivetrain studies [13]; nonlinear dynamics of spur-gear pairs in the frequency domain [14]; collaborative design of cylindrical and skived face gears [15]; learning-based control and optimization in manufacturing [16]; and digital-twin-oriented route optimization [17]. Data-driven structural optimization further reduces computational cost by leveraging neural networks [18].

By combining simplicity, determinism, and high numerical accuracy, the proposed methodology contributes to more effi-

*e-mail: pstrojny@prz.edu.pl

Manuscript submitted 2025-04-16, revised 2025-10-09, initially accepted for publication 2025-10-14, published in November 2025.

cient and cost-effective design processes in mechanical engineering.

Previous approaches, mainly based on heuristic methods and computationally expensive FEM analyses, are characterized by high computational demand and uncertainty of convergence. What is still missing is a universal and deterministic methodology that ensures full coverage of the solution space while remaining easy to implement in any computational environment. This paper aims to address this research gap by developing a selective search method for the optimization of gear parameters.

The contributions of this paper can be summarized as follows:

- Development of a universal, deterministic algorithm for spur gear optimization based on selective parameter search.
- Precise numerical modeling of tooth geometry, validated against CAD-based generating simulations and FEM analysis.
- Demonstration of high accuracy (error below 1.7%) combined with negligible computational cost, enabling rapid optimization at early design stages.
- Indication of adaptability to other gear types (helical, planetary) and broader machine elements, as well as potential integration with AI-assisted optimization and digital twins.

By combining simplicity, determinism, and high numerical accuracy, the proposed methodology contributes to more efficient and cost-effective design processes in mechanical engineering.

It should be emphasized that the proposed methodology has been verified exclusively by numerical simulations. The lack of experimental validation represents the current limitation of this study and will be the subject of future research.

2. CONSTRUCTION OF THE MATHEMATICAL MODEL OF GEAR GEOMETRY

The geometry of the gear teeth was developed based on the equations of the involute (1) and the extended involute (2). The transition curve (2) is formed as a result of the generating material-removal process using the broaching method with a rack-type tool (Fig. 1).

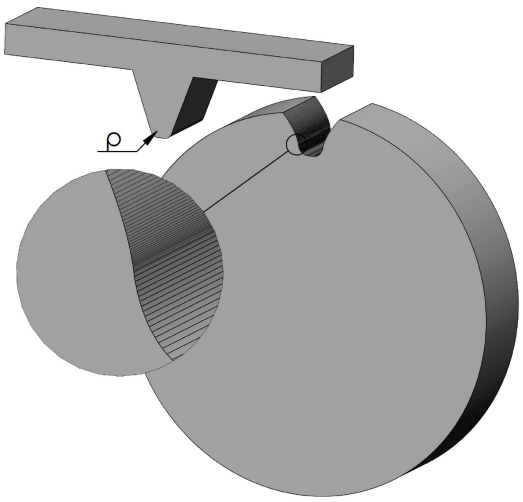

Fig. 1. Schematic of the simulation process for generating material removal using a rack tool, broaching method

2.1. Involute of the working flank

The parametric equation of the involute describing the working flank of the tooth is given by (1). This curve defines the theoretical contact surface ensuring conjugate meshing.

$$\begin{aligned} x(t) &= R_b\big(\sin(t) - t\cos(t)\big), \\ y(t) &= R_b\big(\cos(t) + t\sin(t)\big), \end{aligned} \tag{1}$$

where R_b – base radius, t – roll angle.

2.2. Orientation of the involute in the gear coordinate system

To correctly orient the tooth flank relative to the coordinate system, the involute (1) must be rotated by an angle ξ, which is the sum of angles η and ε (Fig. 2).

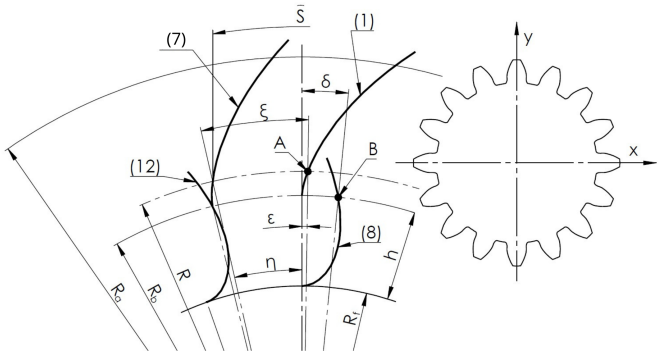

Fig. 2. System of curves used for the construction of the tooth profile: (1) – involute, (8) – extended involute, (7) – involute offset by the tool radius ρ and rotated to the final position, (12) – transition curve with the tool radius ρ taken into account, rotated to the final position. Point A – intersection of curve (1) with the pitch circle, point B – intersection of curve (8) with the base circle. Angles η, ε, and δ illustrate successive geometric transformations

Angle η is expressed by the relation

$$\eta = \frac{s}{2R}, \tag{2}$$

where s – tooth pitch, equal to the quotient of the tooth module and $\pi/2$, R – pitch radius (Fig. 2).

To estimate the angle ε, it is necessary to determine point A (Fig. 2), which is the intersection of the involute (1) with the pitch diameter R (3)

$$t = \sqrt{\frac{R^2}{R_b^2} - 1}\,. \tag{3}$$

As a result, the coordinates of point A and the angle ε are as follows:

$$\begin{aligned} x_A(t) &= R_b\big(\sin(t) - t\cos(t)\big), \\ y_A(t) &= R_b\big(\cos(t) + t\sin(t)\big), \end{aligned} \tag{4}$$

$$\varepsilon = \operatorname{atan}\left(\frac{x_A}{y_A}\right). \tag{5}$$

Ultimately, by using the rotation matrix (6), we obtain the final equation of the tooth flank (7)

$$\begin{bmatrix} x_{A'} \\ y_{A'} \end{bmatrix} = \begin{bmatrix} \cos(\zeta) & -\sin(\zeta) \\ \sin(\zeta) & \cos(\zeta) \end{bmatrix} \begin{bmatrix} x_A \\ y_A \end{bmatrix}, \tag{6}$$

$$\begin{aligned} x_{A'}(t) &= \big(R_b\big(\sin(t) - t\cos(t)\big)\big)\cos(\zeta) \\ &\quad - \big(R_b\big(\cos(t) + t\sin(t)\big)\big)\sin(\zeta), \\ y_{A'}(t) &= \big(R_b\big(\sin(t) - t\cos(t)\big)\big)\sin(\zeta) \\ &\quad + \big(R_b\big(\cos(t) + t\sin(t)\big)\big)\cos(\zeta). \end{aligned} \tag{7}$$

2.3. Extended involute

The parametric equation of the extended involute describes the transition curve at the tooth root (Fig. 2).

$$\begin{aligned} x_w(t) &= R\big(\sin(t) - t\cos(t)\big) - h_r\sin(t), \\ y_w(t) &= R\big(\cos(t) + t\sin(t)\big) - h_r\cos(t), \end{aligned} \tag{8}$$

where h_r – segment equal to the distance $R - R_f$, R_f – root radius of the tooth.

2.4. Tool radius correction

To precisely determine bending stresses at the tooth root, the radius of curvature of the cutting tool (Fig. 1) was considered in the computational algorithm. Consequently, (8) must be shifted along the normal to its curvature by the value ρ, calculated using the derivatives of the components of the parametric equation, which can generally be written as (9)

$$\begin{aligned} x_{w'}(t) &= x_w(t) - \rho\frac{y'_w(t)}{\sqrt{(x'_w(t))^2 + (y'_w(t))^2}}, \\ y_{w'}(t) &= y_w(t) + \rho\frac{x'_w(t)}{\sqrt{(x'_w(t))^2 + (y'_w(t))^2}}. \end{aligned} \tag{9}$$

2.5. Vertical correction of the transition curve

Additionally, to accurately position the equation relative to the tooth system, it must be shifted vertically by the value ρ, resulting in equation (10).

$$\begin{aligned} x_{w''}(t) &= \frac{R\big(\sin(t) - t\cos(t)\big) - h_r\sin(t) + }{\sqrt{\big(R\big(\cos(t) - t\sin(t)\big) - h_r\cos(t)\big)^2 + }} \\ &\quad \frac{+\rho\big(R\big(\sin(t) - t\cos(t)\big) + h_r\sin(t)\big)}{+\big(-R\big(\sin(t) + t\cos(t)\big) + h_r\sin(t)\big)^2}, \\ y_{w''}(t) &= \frac{R\big(\cos(t) + t\sin(t)\big) - h_r\cos(t) + }{\sqrt{\big(R\big(\cos(t) - t\sin(t)\big) - h_r\cos(t)\big)^2 + }} \\ &\quad \frac{+\rho\big(R\big(\cos(t) - t\sin(t)\big) - h_r\cos(t)\big)}{+\big(-R\big(\sin(t) + t\cos(t)\big) + h_r\sin(t)\big)^2}. \end{aligned} \tag{10}$$

To correctly generate the lateral tooth surface, the transition curve (10) must be rotated by the sum of angles ξ and δ. Angle ξ, defined as the sum of η (2) and ε (5), was previously calculated for the rotation of curve (1), resulting in curve (7). However, due to the mathematical complexity of curve (10), the analytical determination of angle δ is extremely difficult, so a numerical method was used. Figure 3 presents the scheme for numerically determining angle δ using universal loops and logical conditions. The method is based on the numerical determination of point B (Fig. 2), representing the intersection of the transition curve (8) with the base radius R_b.

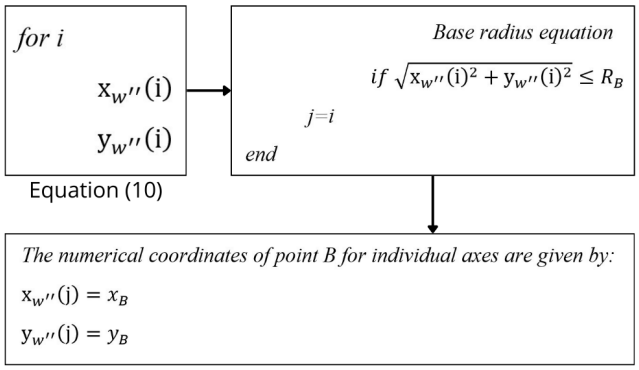

Fig. 3. Numerical algorithm for determining point B – the intersection of the transition curve with the base circle R_b. The resulting coordinates (x_B, y_B) are used to calculate angle δ and correctly position the transition curve

2.6. Numerical determination of angle δ

With the coordinates of point B, angle δ can be determined (11)

$$\delta = \operatorname{atan}\left(\frac{x_B}{y_B}\right). \tag{11}$$

2.7. Final rotated transition curve

Finally, using the value of angle δ and applying the rotation matrix, the equation of the transition curve takes the form (12).

$$\begin{aligned} x_{w''}(t) = &\Bigg(R\big(\sin(t) - t\cos(t)\big) - h_r\sin(t) \\ &+\rho\frac{R\big(\sin(t) + t\cos(t)\big)}{\Big(\sqrt{\big(R\big(\cos(t) - t\sin(t)\big) - h_r\cos(t)\big)^2}} \\ &\frac{-h_r\sin(t)}{+\big(-R\big(\sin(t) + t\cos(t)\big) + h_r\sin(t)\big)\big)^2}\Bigg)\cos(\delta) \\ &-\big(R\big(\cos(t) + t\sin(t)\big) - h_r\cos(t) \\ &+\rho\frac{R\big(\cos(t) - t\sin(t)\big)}{\Big(\sqrt{\big(R\big(\cos(t) - t\sin(t)\big) - h_r\cos(t)\big)^2}} \\ &\frac{-h_r\cos(t)}{+\big(-R\big(\sin(t) + t\cos(t)\big) + h_r\sin(t)\big)\big)^2}\Bigg)\sin(\delta + \xi), \end{aligned} \tag{12a}$$

$$y_{w''}(t) = \left(R\big(\sin(t) - t\cos(t)\big) - h_r \sin(t) + \rho \frac{R\big(\sin(t) + t\cos(t)\big)}{\left(\sqrt{\big(R\big(\cos(t) - t\sin(t)\big) - h_r \cos(t)\big)^2}\right)} \frac{-h_r \sin(t)}{+\big(-R\big(\sin(t) + t\cos(t)\big) + h_r \sin(t)\big)^2} \right) \sin(\delta) - \big(R\big(\cos(t) + t\sin(t)\big) - h_r \cos(t) + \rho \frac{R\big(\cos(t) - t\sin(t)\big)}{\left(\sqrt{\big(R\big(\cos(t) - t\sin(t)\big) - h_r \cos(t)\big)^2}\right)} \frac{-h_r \cos(t)}{+\big(-R\big(\sin(t) + t\cos(t)\big) + h_r \sin(t)\big)^2} \right) \cos(\delta + \xi). \quad (12b)$$

By applying an analogous numerical method, the final length of curve (7) can be determined by its intersection with the addendum radius R_a, and the length of curve (12) by its intersection with the base radius R_b.

2.8. Verification of geometry

To verify the correctness of the above equations, a plot was generated (Fig. 4) based on sample input data: $m = 4$ mm, $z = 16$, $\rho = 1.5$ mm, and compared with the geometry obtained from the generating simulation of the broaching process. The simulation method involves iterative subtraction of the tool volume from the envelope volume, resulting in a faceted tooth structure (Fig. 1).

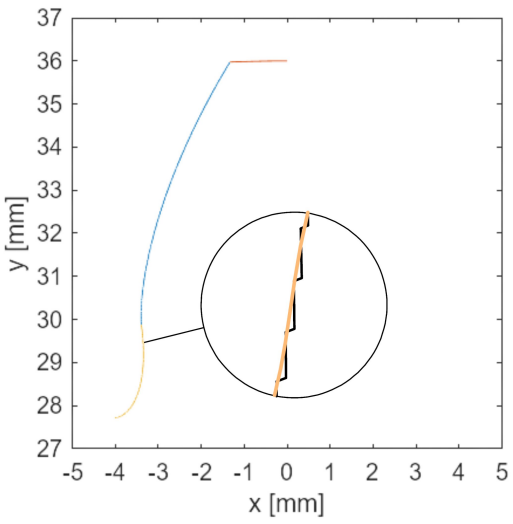

Fig. 4. Example tooth geometry derived from equations (7) and (12) compared with the geometry obtained from the broaching simulation

Figure 4 shows that the curves obtained by both methods virtually coincide. The only difference is the faceting effect visible in the broaching simulation. The obtained convergence confirms the correctness of the above equations describing the curves that form the tooth flank.

3. ANALYSIS OF BOUNDARY CONDITIONS OF THE OPTIMIZED GEAR TRANSMISSION

3.1. Structural and strength constraints

For effective gear optimization, it is necessary to introduce a set of structural and strength constraints: contact ratio (13), contact stress (14), and root stress (15).

Contact ratio:

$$\varepsilon_\alpha = z_1 \left(\frac{1}{2\pi} \sqrt{\left(1 + \frac{2h_{a1}}{2R_1}\right)^2 \frac{1}{\cos^2 \alpha} - 1} \right) + z_2 \left(\frac{1}{2\pi} \sqrt{\left(1 + \frac{2h_{a2}}{2R_2}\right)^2 \frac{1}{\cos^2 \alpha} - 1} \right) - \frac{(R_1 + R_2)\sin\alpha}{\pi m \cos\alpha}, \quad (13)$$

where z_1, z_2 – number of teeth of the mating gears, h_{a1}, h_{a2} – addendum height, equal to $R_{a1,2} - R_{1,2}$, α – pressure angle, m – gear module.

Contact stress:

$$p = \sqrt{\frac{2F}{b\left(\frac{1}{E} + \frac{1}{E}\right)} \left(\frac{1}{R_{b1}\tan(\alpha)} + \frac{1}{R_{b2}\tan(\alpha)} \right) \frac{1}{2\pi(1-\nu^2)}}, \quad (14)$$

where F – resultant tangential force, E – Young's modulus, R_{b1}, R_{b2} – base radii of the mating gears, ν – Poisson's ratio, b – face width of the gear.

3.2. Numerical determination of root stresses using the rectangle method

One of the biggest challenges in strength calculations is the determination of stresses at the tooth root. This is particularly difficult for gears with a small number of teeth due to the concave shape of the root transition curve (Fig. 5), which complicates

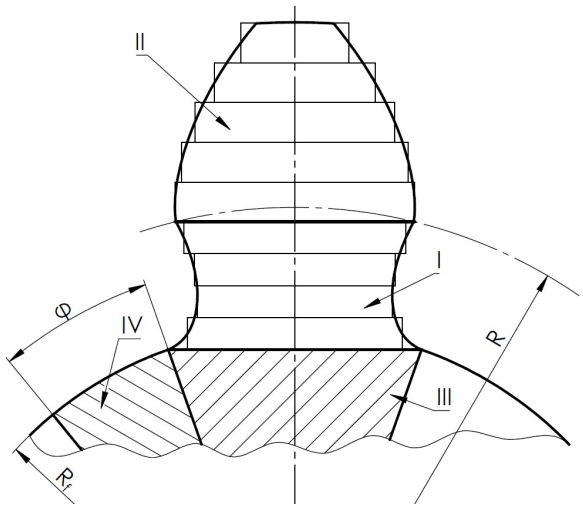

Fig. 5. Diagram of region sets for strength analysis and volume measurements of the rack: I – tooth root, II – tooth tip, III – area directly under the tooth, IV – area directly under the root fillet

the estimation of both the narrowest section of the root and the radius at which the bending force acts (15).

$$\sigma = \frac{6F_R r_y(h_b)}{bh(h_b)^2}, \tag{15}$$

where σ – bending stress, F_R – tangential force, b – tooth width, $r_y(h_b)$ – lever arm of the tangential force as a function of the height along the root curve, $h(h_b)$ – tooth width as a function of the height along the root curve.

To accurately determine bending stresses, numerical integration was employed. The working part of the tooth was divided into rectangles inscribed within area I, as illustrated in Fig. 5. Based on the algorithm (described in detail in Section 3), which uses numerical loops, the root stresses were computed. To verify the accuracy of the results obtained, FEM analysis (Fig. 6) was conducted for five representative examples. The FEM analysis parameters are presented in Table 1. Figure 7 shows the stress distribution along the root transition curve with an indicated peak value. Tooth parameters for the data shown in Fig. 7 were as follows: torque – $M = 1270$ Nm, module – $m = 30$ mm, number of teeth – $z = 9$, face width – $b = 30$ mm, tool rounding radius – $\rho = 1$ mm.

Table 1
FEM analysis parameters for the presented model

Max. element size [mm]	2
Min. element size [mm]	1
Total nodes [–]	5375
Total elements [–]	2596
Jacobian points [–]	16
Min. elements per circle [–]	8
Element growth rate [–]	1.4
Stress [MPa]	Mises

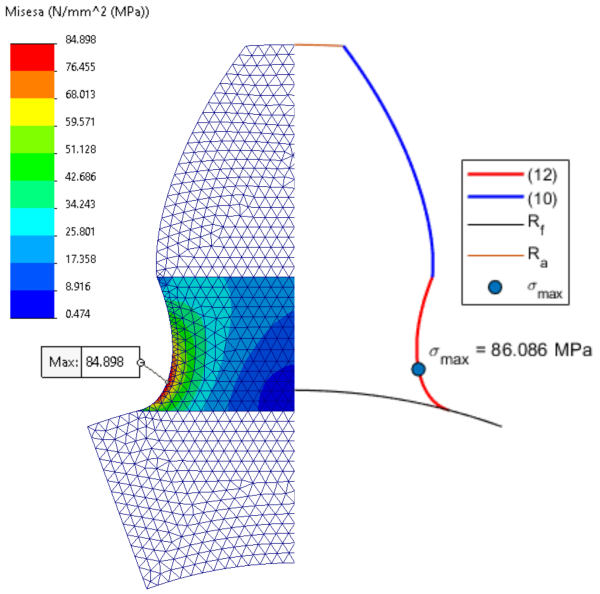

Fig. 6. Results of strength analysis for root stresses using FEM. The left part of the figure shows the stress map obtained from FEM with the location of maximum stresses indicated, while the right part presents the tooth flank profile with the maximum stress point determined by the numerical optimization method

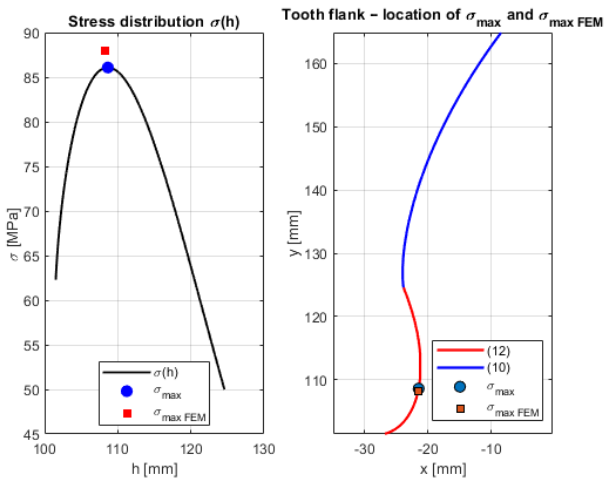

Fig. 7. Stress distribution along the root transition curve: $\sigma(h)$ – stress distribution from numerical analysis, $\sigma_{\max}$ – maximum stress from numerical analysis, $\sigma_{\text{max-FAM}}$ – maximum stress from FEM analysis

A more detailed comparison of the results is provided in Section 5.2.

3.3. Construction of the objective function based on a numerical method

In the analyzed case, the objective function corresponds to the sum of the volumes of sectors I, II, III, and IV in Fig. 5, where the volumes of sectors I and II were determined numerically based on equations (7) and (12), respectively. Volumes III and IV are described by equations (15) and (16), respectively.

$$V_3 = \left(\frac{1}{2}R_f^2 \sin(2\delta)\right) zb, \tag{16}$$

$$V_4 = \left(R_f^2(\pi - z\delta)\right) b. \tag{17}$$

It is important to emphasize that in this case, volume is equivalent to mass, as the material density is assumed to be constant.

4. ALGORITHM FOR THE NUMERICAL METHODOLOGY OF GEAR PARAMETER OPTIMIZATION

To optimize gear transmission, an algorithm was developed, as illustrated in Fig. 8. The algorithm is based on six steps. In the first step, the necessary gear parameters are provided. The second step involves generating a set of decision variables, which either change according to a specified accuracy increment or are selected from standardized tabulated values (such as module and pressure angle). The third step eliminates those variable combinations that do not meet the constraint conditions described

in Section 3 (3.1, 3.2). In step four, an *n*-dimensional feasible solution space is constructed, where n corresponds to the number of decision variables. Step five involves searching the entire feasible solution space to identify the single best solution in accordance with the objective function defined in Section 3.3. Finally, step six presents the results of the optimal gear configuration, which satisfies all predefined constraints and achieves the lowest possible mass.

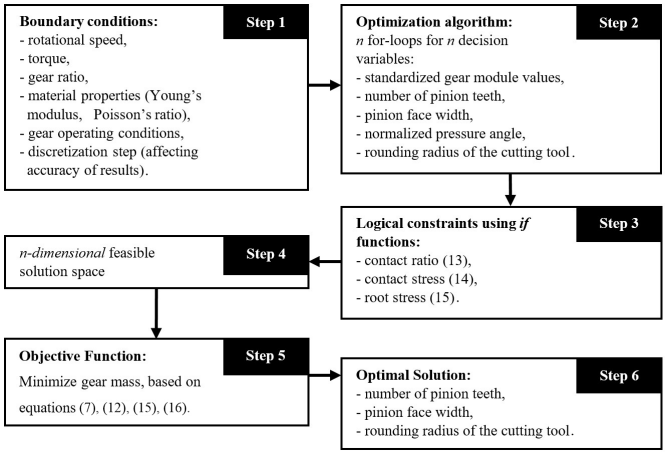

Fig. 8. Flowchart of the optimization algorithm for gear parameter selection

5. RESULTS AND DISCUSSION

To validate the correctness of the presented algorithm (Fig. 8), a series of analyses was conducted to verify the accuracy of the generated geometry, the estimated mass, and the values and distribution of root stresses.

5.1. Comparison of gear volumes generated by different methods

A comparison was made between five representative pinions generated using a CAD model (Fig. 1) based on the generating simulation of the cutting process, and those generated using the optimization algorithm (Fig. 8). The results are presented in Table 2.

Table 2

Comparison of pinion volumes generated by the envelope simulation method (Fig. 1) and by the optimization algorithm (Fig. 8)

No.	Module [mm]	Number of teeth [–]	Face width [mm]	Tool radius [mm]	Volume from optimization algorithm [mm^3]	Volume from CAD model [mm^3]	% Difference
1	30	9	30	2	1693408.48	1693564.69	0.01%
2	20	14	15	2	916953.55	917029.27	0.0083%
3	10	19	25	1	705898.31	706349.91	0.06%
4	5	24	30	1	338310.27	338351.23	0.02%
5	2	29	35	0	92253.17	92203.32	0.05%

As seen in Table 2, the differences between the results obtained by the two methods do not exceed 0.07%. The accuracy of the results is not affected by module size or number of teeth. The analysis was conducted with a discretization step of 0.001 mm.

5.2. Strength analysis of root stresses for five representative pinions

Table 3 compares the results obtained using the algorithm from Fig. 8 and FEM analysis.

Table 3

Comparison of maximum root stresses obtained via the optimization algorithm (Fig. 8) and FEM analysis

No.	Module [mm]	Number of teeth [–]	Face width [mm]	Tool radius [mm]	Torque [Nm]	Max. stress – optimization algorithm [MPa]	Max. stress – FEM [MPa]	% Difference
1	30	9	30	2	1400	92.203	91.59	0.67%
2	20	14	15	1.5	650	93.824	93.358	0.50%
3	10	19	25	1	420	93.089	92.459	0.68%
4	5	24	30	0.5	165	90.053	91.258	1.34%
5	2	29	35	0.2	38	90.862	89.369	1.64%

As shown in Table 3, the differences between the algorithmic results and FEM analyses did not exceed 1.7%, regardless of module size or number of teeth, which confirms the reliability of the method. At the same time, the selective search algorithm provided sub-micron resolution with negligible computational overhead: a single optimization run required only 25–30 seconds, compared to 15–18 minutes for an equivalent FEM-only optimization on the same workstation (Intel i7, 16 GB RAM). This corresponds to more than a 30-fold reduction in computational cost while maintaining engineering-level accuracy, making the method particularly valuable at the early design stage where multiple design variants must be assessed quickly.

In addition, a preliminary sensitivity analysis was conducted, showing that small variations in input parameters (such as module or tool radius) do not significantly affect the results of stresses and geometry. This confirms the stability of the algorithm and its robustness against numerical errors. In future work, the methodology will be complemented with a full statistical error analysis to quantitatively define uncertainty ranges.

Compared to heuristic algorithms such as genetic algorithms, simulated annealing, or Bayesian optimization, the proposed selective search method is fully deterministic. This guarantees complete coverage of the feasible design space and minimizes the risk of being trapped in local minimum, while metaheuristics are inherently probabilistic and may produce different results in repeated runs.

The methodology is particularly attractive for applications requiring lightweight and reliable transmission systems, such as automotive gearboxes, aerospace actuators, and robotic drive systems, where rapid evaluation of multiple design variants with engineering-level accuracy is critical.

Moreover, the deterministic structure of the algorithm facilitates its adaptation beyond spur gears. With minor modifications of the geometric model, the methodology can be extended to helical and planetary gears, as well as other machine elements (e.g., splines, shafts). This flexibility, combined with high computational efficiency, highlights the potential of the selective search method as a universal tool for machine design optimization.

5.3. Contact ratio and contact stress

The remaining strength criteria (13) and (14) were explicitly implemented into the algorithm. The results obtained using numerical loops and logical conditions are entirely consistent with analytical solutions.

The minimal discrepancies between the results obtained via different methods support the assumption that the presented algorithm is valid and the results are correct.

6. CONCLUSIONS

This study deliberately omitted the analysis of certain parameters, such as tip clearance, backlash, profile correction, addendum height, and the influence of the root cutting method since their impact on gear optimization represents an area for future research and will be the subject of subsequent publications. Their inclusion could significantly affect tooth strength and durability, making them important directions for further investigation.

The developed method enables extremely rapid optimization of spur gear transmissions. The presented algorithm, based on universal loops and logical conditions, is characterized by ease of implementation in any numerical computation software. Moreover, the algorithm allows for the flexible addition of further constraints, whether strength-related, technological, or structural, making it highly adaptable to the specifics of the analyzed system. The approach also offers potential for expansion with additional decision variables, such as material type, which further increases the scope and universality of the proposed optimization method.

In summary, the novelty of the proposed algorithm lies in its deterministic and universal structure, enabling adaptation not only to spur gears but also to helical and planetary gears, as well as other machine elements. Its practical applications include automotive transmissions, lightweight aerospace gearboxes, and robotic drive systems. Future research directions include integration with AI-assisted optimization, digital twin concepts, sustainable design strategies, and the inclusion of sensitivity analysis, statistical error assessment, and industrial factors such as manufacturing time and production costs. Together, these aspects will further broaden the relevance and applicability of the method in engineering practice.

REFERENCES

[1] J. Kochańska, A. Burduk, D. Łapczyńska, and K. Musiał, "The solution of MRSLP with the use of heuristic algorithms," *Bull. Pol. Acad. Sci. Tech. Sci.*, vol. 72, no. 1, p. e146407, 2024, doi: 10.24425/bpasts.2024.146407.

[2] E. Aslan, "Prediction and comparative analysis of emissions from gas turbines using random search optimization and different machine learning-based algorithms," *Bull. Pol. Acad. Sci. Tech. Sci.*, vol. 72, no. 6, p. e151956, 2024, doi: 10.24425/bpasts.2024.151956.

[3] M. Baranowski, G. Fotyga, A. Lamecki, and M. Mrozowski, "Bayesian optimization for solving high-frequency passive component design problems," *Bull. Pol. Acad. Sci. Tech. Sci.*, vol. 70, no. 4, p. e141595, 2022, doi: 10.24425/bpasts.2022.141595.

[4] M. Łoś, M. Woźniak, and M. Paszyński, "Varying coefficients in parallel shared-memory variational splitting solvers for non-stationary Maxwell equations," *Bull. Pol. Acad. Sci. Tech. Sci.*, vol. 72, no. 3, p. e149179, 2024, doi: 10.24425/bpasts.2024.149179.

[5] G. Peruń, "The use of dynamic modeling for optimization of machine design on the example of a toothed gear," *Vibr. Phys. Syst.*, vol. 33, no. 3, p. 2022322, 2022, doi: 10.21008/j.0860-6897.2022.3.22.

[6] P. Strojny, "Modification of the Tooth Geometry of a Polymer GEAR with a Straight Tooth Line to Adjust the Torque Transmission Capability in One Direction Only," *Tech. Sci. Univ. Warmia and Mazury Olsztyn*, vol. 24, no. 1, pp. 157–170, 2021, doi: 10.31648/ts.6914.

[7] P. Strojny, "Optimization of the hub-ring gear connector using modern numerical methods," *Przegl. Mech.*, vol. 2021, no. 4, pp. 18–22, 2021.

[8] M. Zajdel *et al.*, "Geometrical accuracy of injection-molded composite gears," *Polimery*, vol. 67, no. 7–8, pp. 324–336, 2022, doi: 10.14314/polimery.2022.7.5.

[9] M. Zhang, C. Xu, D. Xu, G. Ma, H. Han, and X. Zong, "Research on improved sparrow search algorithm for PID controller parameter optimization," *Bull. Pol. Acad. Sci. Tech. Sci.*, vol. 71, no. 6, p. e147344, 2023, doi: 10.24425/bpasts.2023.147344.

[10] M. Nowak and A. Boguszewski, "Topology optimization without volume constraint – the new paradigm for lightweight design," *Bull. Pol. Acad. Sci. Tech. Sci.*, vol. 69, no. 4, p. e137732, 2021, doi: 10.24425/bpasts.2021.137732.

[11] J. Yao, J. Wang, Q. Mao, and Y. Yang, "Optimization of Plasma Welding Sequence and Performance Verification for a Fork Shaft: A Comparison of Same-Direction and Reverse-Direction Welding," *Materials*, vol. 18, no. 2, p. 288, 2025, doi: 10.3390/ma18020288.

[12] X. Sun, Z. Qian, Y. Xu, and J. Huang, "Meshing Characteristic Analysis of CBR Reducer Considering Tooth Modification and Manufacturing Error," *Machines*, vol. 12, no. 12, p. 915, 2024, doi: 10.3390/machines12120915.

[13] R. Jakubowski and P. Jakliński, "A Practical Approach to Modeling and Performance Analysis of a Turboshaft Engine Using Matlab," *Appl. Sci.*, vol. 14, no. 23, p. 1373, 2024, doi: 10.3390/app142311373.

[14] G. Saletti, G. Battiato, and S. Zucca, "A Coupled Harmonic Balance-Based Approach for the Non-Linear Dynamics of Spur-Gear Pairs," *Vibration*, vol. 8, no. 2, p. 18, 2025, doi: 10.3390/vibration8020018.

[15] Z. Zhou *et al.*, "A Collaborative Design Method for the Cylindrical Gear Paired with Skived Face Gears Driven by Contact Performances," *Mathematics*, vol. 13, no. 7, p. 1180, 2025, doi: 10.3390/math13071180.

[16] D. Kalandyk, B. Kwiatkowski, and D. Mazur, "CNC machine control using deep reinforcement learning," *Bull. Pol. Acad. Sci. Tech. Sci.*, vol. 72, no. 3, p. e148940, 2024, doi: 10.24425/bpasts.2024.148940.

[17] Z. Chen, J. Zou, and W. Wang, "Digital twin-oriented dynamic optimization of multi-process route based on improved hybrid ant colony algorithm," *Bull. Pol. Acad. Sci. Tech. Sci.*, vol. 72, no. 3, p. e148875, 2024, doi: 10.24425/bpasts.2024.148875.

[18] X. Kong, Y. Wu, P. Zhu, P. Zhi and Q. Yang, "Novel Artificial Neural Network Aided Structural Topology Optimization," *Appl. Sci.*, vol. 14, no. 23, p. 11416, 2024, doi: 10.3390/app142311416.